

# System identification estimation of soil properties at the Lotung site

S.D. Glaser\*, L.G. Baise

*Department of Civil and Environmental Engineering, University of California, 440 Davis Hall, Berkeley, CA 94720, USA*

Received 29 January 2000; accepted 17 March 2000

## Abstract

Dynamic properties of the soils at the Lotung test site, Lotung, Taiwan, are estimated from seismic vertical array measurements (input–output data sets) using both time-invariant and time-variant parametric modeling methods (system identification). Soil properties are directly mapped from model parameters to an equivalent lumped mass model of the soil interval. Shear stiffness and damping ratios were calculated for 8 events with  $M_L$  ranging from 4.5 to 7.0. Shear stiffness ranged between 0.5 and 6 MN/m, inversely proportional to PGA. The equivalent viscous damping ratio varied from 2 to 30% of critical damping, proportional to PGA. Degradation of soil behavior, while less pronounced with increasing depth, consistently occurs above a peak input acceleration of 0.07 g. Although “non-linear” behavior is evident above 0.17 g, Event 7 (0.21 g) is accurately predicted using a linear constant parameter model estimated from the smaller Event 8 aftershock ground motions. © 2000 Elsevier Science Ltd. All rights reserved.

*Keywords:* Damping; Earthquake engineering; In situ testing; Non-destructive estimation; System identification; Stiffness; Time series

## 1. Introduction

There are many unanswered questions of interest to the geotechnical community, concerning the behavior of soils subjected to earthquake excitation. Foremost among them are questions concerning the strain-dependent non-linear behavior of soils, and soil–structure interaction (SSI). This paper makes use of the Lotung Large-Scale Testing (LSST) site data set and system identification analyses to develop reliable shear stiffness and damping estimates for a wide scale of earthquake-induced strain. The Lotung strong motion data set is a unique set of data encompassing a wide range of shaking intensity, hence displacements. The completeness of this input–output data set makes it ideal for analysis using system identification (SI) methods, a formalized inverse method. A full geotechnical report of the site can be found in Anderson [1] or Anderson and Tang [2].

Soil response to both small (peak ground acceleration (PGA) < 0.07 g) and large (PGA > 0.17 g) earthquake excitations are analyzed. In particular, estimates of soil damping and stiffness are made for a suite of earthquakes recorded at the Lotung array using a simple lumped mass model to represent the soil system. Although the lumped mass model is not the “best” or most perfect constitutive

model for wave propagation through soil, it is a commonly used and a consistent simplification. In addition, the lumped mass model can be easily inverted for using standard SI methods. By studying the changes in the equivalent linear models most appropriate for different levels of ground excitation, estimates of non-linear soil behavior can be given. Soil response from the smaller events allows characterization of time-invariant, linear, small strain behavior of different soil intervals (soil horizon between accelerometer stations), and serves as a baseline response. For the large events, which induce larger displacements in the soil, recursive SI methods are used to estimate the soil system behavior as it changes through time. The time-varying estimates of soil behavior during the large events illustrate the non-linearity of soil when subjected to large displacements.

### 1.1. Why use system identification?

An important goal for geotechnical engineers is the ability to estimate soil properties without the measurement process disturbing the soil mass. In as much as an earthquake can be considered non-destructive, the archetypal large displacement excitation is earthquake strong motion, and the resultant soil motions are routinely recorded. At sites with installed vertical arrays, both ground motions into the bottom of the soil layer of interest, and out of the top of this layer are recorded, as illustrated by the cartoon in Fig. 1 (assuming 1D vertical wave propagation). Given this known

\* Corresponding author. Tel.: +1-510-642-1264; fax: +1-510-642-7476.  
E-mail address: glaser@ce.berkeley.edu (S.D. Glaser).

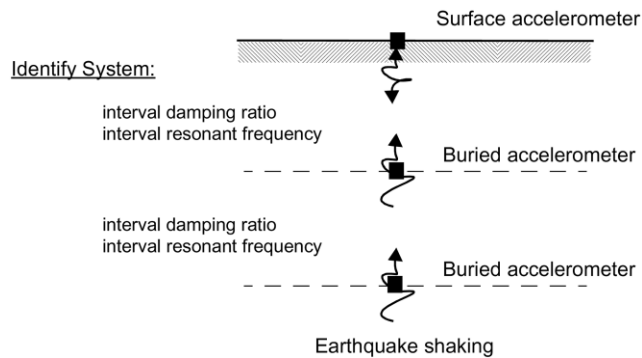


Fig. 1. Configuration of the system identification method.

input propagating upward from depth, and the output at the top of each horizon of the soil column, the behavior of the soil at each interval between accelerometers can be modeled by inverse theory. If a suitable model is chosen to represent the system of interest, the estimated model parameters will correspond to important mechanical parameters of the chosen model system, such as stiffness and equivalent viscous damping ratio. This estimation of parameters is commonly known as SI. Previous applications of SI to geotechnical problems include Glaser [3–5], Zeghal et al. [6], Elgamal et al. [7], and Stewart et al. [8,9]. Parametric modeling, commonly used in automatic control, evolved into the field of adaptive filtering that has been developed to calculate parameter estimates for a system as properties vary over time. Therefore, adaptive filtering offers a tremendous advantage for analyzing soil systems as the displacements increase and the soil system behavior transforms from effectively linear to overwhelmingly non-linear.

## 2. The Lotung site, Taiwan

With increasing use of nuclear-powered generating plants in the 1970s, many safety-related questions about the seismic performance of these plants arose. In the early 1980s, the Electric Power Research Institute (EPRI) and the Taiwan Power Co. constructed two scale models (1/4 and 1/12 scale) of a nuclear containment structure near Lotung, Taiwan, seismically a very active area in northeast Taiwan. The site and structures were elaborately instrumented so that soil and structural response, and SSI could be carefully studied during earthquakes [10].

### 2.1. Instrumentation

The soil instrumentation at the LSST site includes a three-arm surface array with arms radiating approximately 49 m from the 1/4 scale containment structure [11]. In addition, there are two downhole arrays of accelerometers extending to a depth of 47 m. The surface sensors are triaxial force-balance units (Kinometrics FBA-13) oriented in the N–S, E–W, and vertical directions. The downhole arrays (DHA

and DHB) are modified Kinometrics FBA-13H units oriented in the N–S, E–W, and vertical directions. DHA is located 3 m from the 1/4 scale structure and DHB is located 49 m from the structure, allowing identification of the effects of the structure on soil response. The downhole instruments are located at depths of 6, 11, 17, and 47 m.

### 2.2. Site characterization

The geology of the Lotung site is summarized by Wen and Yeh [12] and Tang [11]. The area consists of a recent alluvium layer 40–50 m thick overlying a Pleistocene formation that varies from 150 to 500 m in thickness. Underlying the Pleistocene material is a Miocene basement rock. A simplified soil profile consists of 30–35 m of silty sand and sandy silt with some gravel, above clayey silt and silty clay. The site has been extensively investigated [1,2] with five independent testing programs.

### 2.3. Seismology

A summary of the properties of measured temblors is given in Table 1. Events 4, 7, 12, and 16 will be considered “large” events, with peak accelerations over 0.17 g. Events 12 and 16 were major events and have been discussed in detail [1,13–15]. Of these four large events, temblors 7 and 16 were deep focus events, and Event 12 was an event occurring nearby at shallow depth. Event 8, although a low acceleration event, is of special interest as it was an immediate aftershock of Event 7. The magnitude of ground shaking is quantified using the peak ground acceleration.

### 2.4. Pore pressure generation

Under static conditions, the water table is within half a meter of the ground surface with an artesian head of about 1.5 m at 6 m deep in the SM layer, and at 60 m deep [16]. The static pore water pressure is approximately 10 kPa/m depth, although there is local variation of  $-1$  and  $+2.5$  kPa/m over the site. As reported [16], numerous mechanical problems hindered the collection of pore pressure data; however, sensors were triggered by Events 12, 16, and 17. Excess pore water pressure was measured in all three events, with the excess pore water pressure rising to 27% of the initial vertical effective stress at a depth of 6.03 m (black, silty, fine sand capped by a low permeability layer) for Event 12 and 25% during Event 16 in the same soil layer.

## 3. Some previous SI studies of the Lotung site

Zeghal et al. [17] used cross-spectral analysis of the data set to calculate resonant frequencies up to the twelfth mode of vibration for the LSST site as a whole. Elgamal et al. [18] in a companion paper, documents a technique for evaluating the soil shear stress–strain histories directly from the downhole acceleration records using linear interpolation between downhole accelerometers. They use the results of the

Table 1  
Properties of the recorded LSST series of earthquakes

Event and date	Epicentral distance (km)	Focal depth (km)	Local magnitude	Peak acceleration (g)	Arias intensity (m/s)
2 (10/26/85)	29.1	1.2	5.3	0.03	–
3 (11/07/85)	16.6	79.0	5.5	0.01	74
4 (01/16/86)	23.7	10.2	6.5	0.49	1845
5 (03/29/86)	8.5	10.3	4.7	0.04	73
6 (04/08/86)	31.4	0.9	5.4	0.04	126
7 (05/20/86)	66.2	15.8	6.5	0.21	652
8 (05/20/86)	69.2	21.8	6.2	0.03	139
9 (07/11/86)	5.0	1.1	4.5	0.07	192
10 (07/16/86)	6.1	0.9	4.5	0.04	36
11 (07/17/86)	6.0	2.0	5.0	0.10	–
12 (07/30/86)	5.2	1.6	6.2	0.20	2710
13 (07/30/86)	–	–	6.2	0.05	161
14 (07/30/86)	4.7	2.3	4.9	0.05	124
15 (08/05/86)	4.7	0.7	4.9	0.05	386
16 (11/14/86)	77.9	6.9	7.0	0.17	3995
17 (11/14/86)	–	–	–	0.04	310
18 (11/15/86)	–	–	–	0.03	91

calculation to estimate the soil damping at different depths as a function of strain amplitude.

Zeghal et al. [17,19] estimated shear moduli and modal damping for a full suite of Lotung events. The study reported much more scatter in estimates of damping than for shear modulus, especially for low strain ( $<3 \times 10^{-3}\%$ ). Damping was found to be at or above the commonly accepted values put forth by Seed and Idriss [20]. Elgamal, however, has reported that the estimated values for damping ratio were extremely sensitive to subtle changes in assumed sensor alignment [21]. For Event 16, which generated an excess pore water pressure equal to about 25% of the effective overburden stress, Elgamal et al. [18] estimated a shear modulus reduction of about 14–17%.

Chang et al. have undertaken a series of studies of Lotung site records using Fourier-based methods to evaluate the non-linear response of soils due to strong motion [13,22–24]. The first phase of the work concentrated on calculating a transfer function for the soil at three different segments of the excitation history. The results from the forward propagation non-linear DESRA-2 analysis [25] show good agreement between actual and calculated displacement for frequencies up to about 6 Hz. The shear modulus reduction factors showed a marked decrease from the initial low-level excitation to peak deformation, ranging from 0.60 to 0.14. The resultant  $G/G_{\max}$  and  $D/D_{\min}$  curves put into context the range of field strain that is best represented by different laboratory tests. This study reported a marked difference between soil properties estimated from East/West and North/South horizontal ground motions.

Further work on the shear modulus reduction curve based on actual large strain measurement was reported by Chang et al. [13,22], using shearing strains estimated by SHAKE [26]. The equivalent  $S$ -wave velocities calculated from the transfer functions are input into the computer program SHAKE, along with damping curves from laboratory tests.

Chang et al. [13] attempts to account for the non-stationarity of the ground motion time histories by dividing the signal into 5 s pseudo-stationary segments and using a 0–12 Hz bandwidth frequency-domain solution using 125 points.

#### 4. Identification methods used in this study

##### 4.1. Parametric modeling

The goal of SI is to invert recorded data to estimate a model of a system, providing needed mechanical information about that system. In this case, the data are input–output pairs of recorded earthquake ground motions, and the system is the intervening soil layers. The most common techniques have evolved from electrical and mechanical engineering, and involve solving the inverse problem for the system transfer function. A simple system model is a ratio of weighted polynomials. The weights are the parameters relating system input and output. Such a model, referred to as an autoregressive-moving average (ARMA) model, is based on discrete time series analysis:

$$y_t = a_1 y_{t-1} + a_2 y_{t-2} + \dots + b_0 x_t + b_1 x_{t-1} + \dots e$$

$$\equiv \left[ \sum_{j=0}^{nb} b_j x_{t-j} + \sum_{k=1}^{na} a_k y_{t-k} \right] + e \quad (1)$$

where  $y_j$  is the actual output data sequence,  $x_j$  is the input sequence,  $t$  is the time step counter,  $e$  is white, exogenous noise, and  $na$  and  $nb$  are the AR and MA orders, respectively. In this analysis of recorded data, we use an ARMA model with the effects of exogenous noise added as an error term. The theory and assumptions behind the method, with emphasis on geo- problems, is reviewed in a paper and reported by the author [4,5], as well as others [27,28].

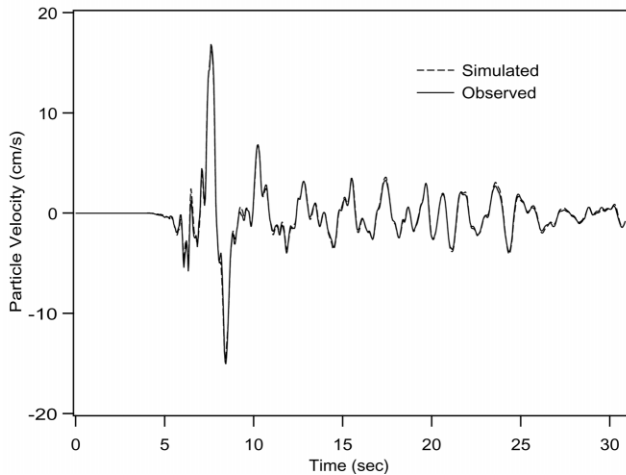


Fig. 2. Comparison of actual and estimated surface velocity time history, Event 12, DHA, 0–6 m interval.

The ARMA model characterizes the time history of earthquake ground motion very well, and has been successfully applied to relevant seismological and structural problems, e.g. [29–31]. Several authors, e.g. [32,33] have proven that seismic transmission through a layered system is an autoregressive process.

A useful method for analyzing changes in the system through time is to use a segmentation scheme, which uses parallel recursive algorithms, to find parametric changes greater than stated error limits, e.g. see Ref. [34]. The segmentation algorithm estimates a sequence of linear models with the segments determined by a set tolerance level. This scheme has the advantage over strictly recursive models of limiting the small-scale parameter fluctuation common in time-variant models, which results from allowing the model to change at each time step. The segmented model only changes after the recursive estimation has consistently indicated model change greater than the tolerance level. A time-step by time-step estimate of the system properties can be made using a full recursive adaptive methodology (RARX), most often with a Kalman filter algorithm [35]. These time-varying methods have proven to be a powerful tool for estimating properties of soil throughout the liquefaction process during the Superstition Hills Earthquake at the Wildlife site [3].

#### 4.2. Mapping of identified model parameters to relevant soil physical properties

In this paper, the system is a given interval of soil lying between pairs of accelerometers. The two mechanical soil properties estimated by this SI process for each vibrational mode are the shear stiffness ( $k_\theta$ ) and equivalent viscous damping ratio ( $\zeta$ ), and are equivalent properties for the entire “effective” layer between the two sensors of interest, idealized as cascaded lumped-mass oscillators. It is not possible to estimate sublayer properties since there is only

one physical realization of the stimulating ground motions (a given earthquake) upon which to invert, and there are an infinite number of combinations that will mathematically satisfy the data. For the same reasons, this paper does not make use of approximate strain estimates ( $\gamma = \dot{u}/V_s$ ) since this “estimate” exists only at the discrete points of measurement rather than for any point between the sensors. The SI estimated parameters are for an entire effective soil interval rather than for discrete points within it.

The SI process described in the proceeding section identifies the weights that map the input time series to the output time series. These parameters were chosen through a mathematically rigorous least squares optimization process for each input–output data set. Given the extreme congruence between actual surface motions and calculated interval outputs (e.g. signal entering the soil layer at 17 and leaving at 11 m), the technique is obviously effective. For example, Fig. 2 is a linear mapping of the north–south velocity motions from Event 12 passing through the 6 m-to-surface layer, a mapping made with just 8 model parameters. This quite ordinary example is close to a perfect fit, and shows that the calculated parameters must be carrying some information about how the soil layer affected the through-passing waveform.

The first mapping in the SI process only involves estimating the weights that make up the ARMA filter, there are still no estimates made for mechanical soil properties. Another mapping — ARMA parameters to soil properties — is needed. An important property of the ARMA model is invoked for soil property estimation — the ARMA difference equation is the difference equation of the integral of the equation of motion of a single degree-of-freedom lumped mass oscillator [27,28]. A  $2n$ - $2n$  ARMA model can therefore easily be mapped to an  $N$ -cascaded single-degree-of-freedom (SDOF) system. The resonant frequency and equivalent viscous damping ratio of the  $N$ -cascaded SDOF oscillators are contained in the  $2n$  AR parameters. Phase relations are preserved in the MA parameters. The resonant frequencies  $f_{vj}$ , percent of critical viscous damping  $\zeta_{vj}$  [27,28] and power participation factor  $P_{vj}$  [36,30] are calculated from the system poles and residues found from the partial-fraction expansion of the Z-transform.

The resonant shear stiffness,  $k_{1\theta}$ , can be calculated from  $f_{vj}$  and  $\zeta_{vj}$  using the definition of resonant frequency. Solving for  $k_{1\theta}$  results in the following equation as a function of fundamental resonant frequency  $f_{r1}$ :

$$k_{1\theta} = \frac{m_1(2\pi f_{r1})^2}{1 - \zeta_{r1}^2} \quad (2)$$

where  $m_1$  is half the layer mass lumped to the “point mass” and half to the base.

The mapping from ARMA parameters to mechanical soil properties is made through the assumption of an  $N$ -cascaded SDOF lumped mass model. The estimated shear stiffness and equivalent viscous damping ratio are the optimal

parameters needed to map the recorded input signal into the recorded output signal through a lumped mass model. An important caveat is that the lumped-mass SDOF model is not an ideal model of the physical soil system, which obviously is a continuous mass system. However, the lumped mass is a commonly accepted model that can offer tremendous insight into complicated dynamic behavior. The lumped-mass idealization is fully as internally consistent as the piece-wise-linear linearization of the wave equation commonly used in geotechnical earthquake engineering, e.g. see Refs. [22,37]. Both approaches regularize non-linear shear modulus behavior through an equivalent damping parameter. With a complicated system such as wave propagation through soil, the large amount of uncertainty makes identifying the “true” system difficult and it is better to estimate a simple equivalent system that also has a physical meaning, such as the lumped mass model.

### 4.3. Choice of model order and validation

The model order and validation was completed according to the procedure set out in Baise and Glaser [39], and Glaser [4]. The procedure relies on minimizing the normalized sum of squared prediction errors without causing overlapping of the poles and zeros of the model, as well as assuring 99% confidence in both the whiteness of the residual auto-correlation and the cross-correlation functions of the input and output residuals [38,40]. Experience has shown that any estimate above the second or third mode is tenuous at best, although numerically we are only limited by computational power as to how many modes we can calculate. Given that the data does not have an infinite signal-to-noise ratio, i.e. there is noise present from many sources including quantization, there is only a limited amount of information that can be taken from the data [41,42]. Additional modes will try to fit the noise rather than the system itself.

If the soil system proved non-linear, the waveforms were analyzed using a recursive Kalman-filter based technique that expressly accounts for non-linearity, e.g. see Refs. [38,43,44]. The recursive algorithm can resolve the changes in the soil parameters; however, the trade-off is added uncertainty in the estimated local values as a result of the estimates being based on fewer data points. While the linear models allowed us to demonstrate trends in soil behavior as a function of peak ground acceleration, the recursive models provided higher resolution of the soil non-linearity through time. The best fit linear ARMA model to actual output for DHA, Event 4, 47–17 m depth is a 12-DOF or 48 parameter model! A simple recursive model, in this case a 3-DOF RARX model, fits the actual data much better. This implies that the system is changing — softening? — through time.

A summary of the estimated fundamental mode  $k_1\hat{\theta}$  for the earthquakes analyzed for this report is given in Table 2, along with corresponding estimates of  $\zeta_{r1}$  for each measured accelerometer interval. These values correspond to the best fit linear ARMA model. The  $k_1\hat{\theta}$ ; and  $\zeta_{r1}$  change little for

small Events 3, 8, 9, and 10. The higher PGA events including Events 4, 7, 12 and 16, with maximum surface accelerations ranging from 0.17 to almost 0.5 g, exhibit consistent decreases in average stiffness from the baseline case. As shown in Fig. 3, when subjected to greater seismic energy the equivalent linear shear stiffness does systematically decrease, while Fig. 4 shows systematic  $\zeta_{r1}$  increase with PGA. When recursive models were used, the parameter estimates were consistent with the linear model values but showed the evolution of estimated properties over the length of the event.

Consider the results from the free field hole, DHB. The average shear stiffness for the 0–6 m interval exhibits a decrease from 5.9 for Events 3, 8, 9, and 10, to 2.4–2.5 MN/m for Events 4, 7, 12 and 16. This result is consistent with the calculations from deeper intervals. The 6–11 m segment shows a decrease from an average of 1.7 for the moderate events to 0.6 MN/m for the larger events. The trend continues to the 11–17 m interval, where the fundamental mode shear stiffness decreases from 1.4 to 0.63 MN/m with increasing shaking intensity. However, the deep interval (17–47 m segment) exhibits virtually no decrease in stiffness with temblor energy. The decrease in fundamental mode shear stiffness and increase in damping with increase in peak input acceleration is readily evident above 17 m depth.

## 5. Discussion

Eight earthquakes of varying characteristics were chosen for this study. The selected temblors represent two classes — strong and mild shaking. The estimated mechanical parameters for the mild (low energy/acceleration) events can be seen as a linear baseline against which to judge whether the larger events exhibited non-linear (softening) behavior. Events 4, 16, and a mainshock and aftershock pair (Events 7 and 8) will be discussed in detail. This section ends with a discussion of SSI for the Lotung site as a whole, and a general discussion on soil damping.

Figs. 3 and 4 graphically compare the correlation of changes in system response (shear stiffness and equivalent viscous damping ratio) to maximum input acceleration. Experience has shown that there is less correlation between system behavior and energy input into soil intervals as measured by Arias Intensity [45]. This leads to a conclusion that soil softening is more a function of peak acceleration (which causes peak displacement) than total input energy (that is proportional to cumulative displacements). This conclusion implies a minimum peak acceleration is needed to excite the soil past its threshold displacement [46].

Effect of confinement is the probable explanation for the lack of change of either shear stiffness or interval damping ratio for the deep interval, 47–17 m. Soil equivalent viscous damping ratio values estimated by this study range from 2 to 33%. The low amplitude event values compare well with

Table 2  
Fundamental mode shear stiffness and viscous damping ratios compared to various earthquake metrics

Earthquake		3		4		7		8		9		10		12		16	
		DH-															
		A	B	A	B	A	B	A	B	A	B	A	B	A	B	A	B
Peak ground acceleration, PGA (g)		0.01		0.49		0.21		0.03		0.07		0.04		0.20		0.17	
Surface arias intensity (m/s)		74		1845		652		139		192		36		2710		3995	
Local magnitude ( $M_L$ )		5.5		6.5		6.5		6.2		4.5		4.5		6.2		7.0	
Vertical array		DH-															
6–0 m	$k_\theta$ (MN/m)	2.4	5.9	1.4	2.3	0.56	2.5	3.1	5.2	–	5.6	–	6.0	1.2	2.5	2.5	2.9
	$\xi$ (% critical damping)	2	5	27	33	18	20	2.4	3	–	2	–	3	13	24	12	18
	Input PGA (g)	0.01	0.01	0.34	0.46	0.11	0.14	0.01	0.01	–	0.02	–	0.04	0.10	0.16	0.11	0.12
11–6 m	$k_\theta$ (MN/m)	1.8	2.1	0.40	0.47	0.49	0.53	1.3	1.7	–	1.8	–	1.7	0.53	0.93	0.77	1.3
	$\xi$ (% critical damping)	5	7	23	28	12	15	5	6	–	6	–	5	16	19	16	20
	Input PGA (g)	0.01	0.05	0.37	0.49	0.09	0.11	0.02	0.002	0.03	0.003	0.03	0.004	0.13	0.16	0.09	0.12
17–11 m	$k_\theta$ (MN/m)	1.4		0.73		0.53		1.41		1.43		1.42		0.43		0.84	
	$\xi$ (% critical damping)	6		33		19		6		10		7		20		17	
	Input PGA (g)	0.01		0.48		0.09		0.02		0.02		0.01		0.19		0.08	
47–17 m	$k_\theta$ (MN/m)	2.1		2.1		1.2		2.1		2.3		2.3		1.3		1.0	
	$\xi$ (% critical damping)	14		16		12		12		12		13		18		14	
	Input PGA (g)	0.01		0.27		0.1		0.01		0.02		0.03		0.22		0.08	
11–0 m	$k_\theta$ (MN/m)	5.0		1.4		–		–		5.1		4.8		4.6		–	
	$\xi$ (% critical damping)	2.3		24		–		–		7		6		12		30	
	Input PGA (g)	0.05		0.49		0.11		0.02		0.03		0.03		0.19		0.1	
47–11 m	$k_\theta$ (MN/m)	3.0		1.26		–		–		2.9		2.5		1.3		1.3	
	$\xi$ (% critical damping)	17		24		–		–		15		13		12		13	
	Input PGA (g)	0.01		0.27		0.1		0.01		0.02		0.03		0.22		0.08	

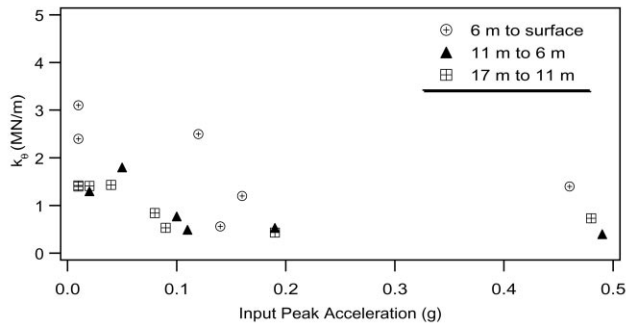


Fig. 3. Effect of peak input acceleration on fundamental mode shear stiffness of each soil interval.

Zeghal et al. [19], but the damping values for Events 7, 12, and 16 are higher than estimated by Zeghal et al. [19]. By comparison with previously reported laboratory damping estimates given in the literature, soil damping estimates presented in this study are greater than values traditionally accepted by geotechnical engineers for forward modeling [20].

5.1. Event 4

Event 4 subjected the Lotung site to the highest peak acceleration of any recorded event in the LSST suite (0.49 g). However, the bore hole was not backfilled at the time of Event 4, leading to some sharp glitches in the data [47]. These few very short but sharp spikes were removed from the data so that this large event could be analyzed and compared to other analyses [17–19,21]. The strong motion for Event 4 was very brief (about 1.6 s) as opposed to Event 16 (about 12 s) and slightly smaller in magnitude ( $M_L = 6.5$  vs. 7.0).

The Event 4 surface layer (6 m to the surface) signal from DHA proved difficult to model using linear techniques, indicating some degree of non-linear behavior that could be better captured using recursive techniques. It was found that the system could be well modeled as a 3-DOF ([6 6 1]) RARX system using a forgetting-factor of 0.83. Fig. 5a shows the congruency between the actual and

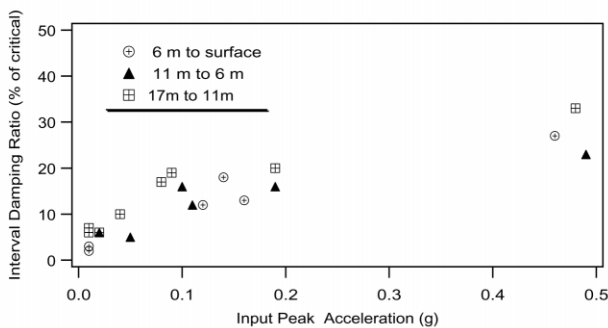


Fig. 4. Effect of peak input acceleration on fundamental mode equivalent viscous damping ratio of each soil interval.

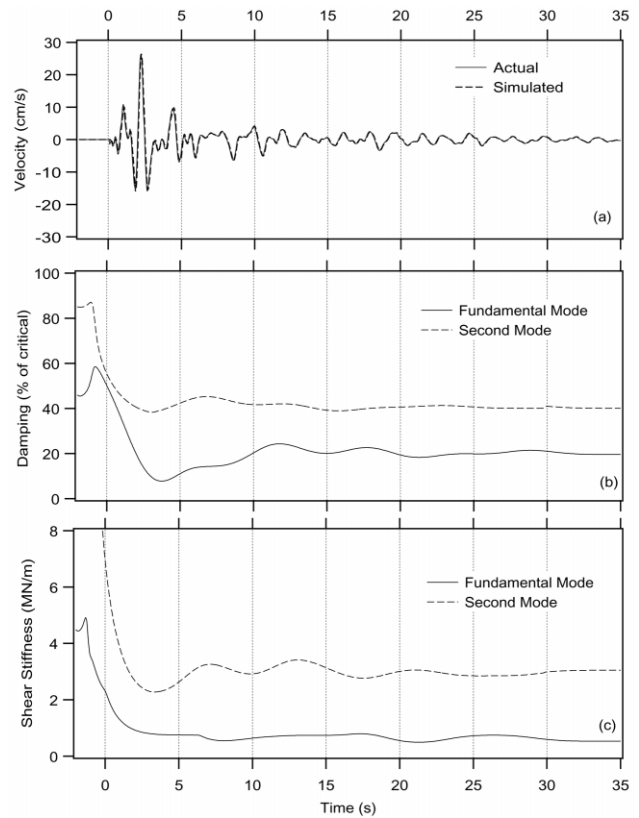


Fig. 5. (a) Comparison of Event 4 simulated and actual velocity history for 6 m to surface, RARX (6 6 1). (b) Evolution of damping ratio,  $\zeta$ , for the fundamental and second mode. (c) Evolution of shear stiffness,  $k_b$ , for the fundamental and second mode.

modeled system, while the evolution of soil damping for the first 2 modes is shown for comparison in Fig. 5b. The recursive model showed a rapid change in parameters during the strong shaking, and then only slight variations throughout the remainder of the event. The recursive model allows time domain resolution at the expense of reduced certainty in the estimates; therefore, the slight undulation in the parameter estimates after the strong shaking can be assumed to suggest constant soil behavior after the initial non-linearity. The evolution of the shear stiffness for the Event 4 surface layer was estimated, and is presented in Fig. 5c. The recursive estimates of shear stiffness and damping ratio are consistent although slightly lower than the values estimated with the linear model, which implies that the estimated parameters using the linear constant parameter model are strongly influenced by the initial very strong motion portion of the data.

5.2. Event 16

Event 16 had the highest magnitude ( $M_L = 7.0$ ) event recorded at Lotung, and also had the greatest Arias intensity (3995 m/s). Pore water pressure rose to 25% of the initial effective vertical stress. Fig. 6a shows the excellent fit for Event 16, 6 m-to-surface interval using a time-invariant

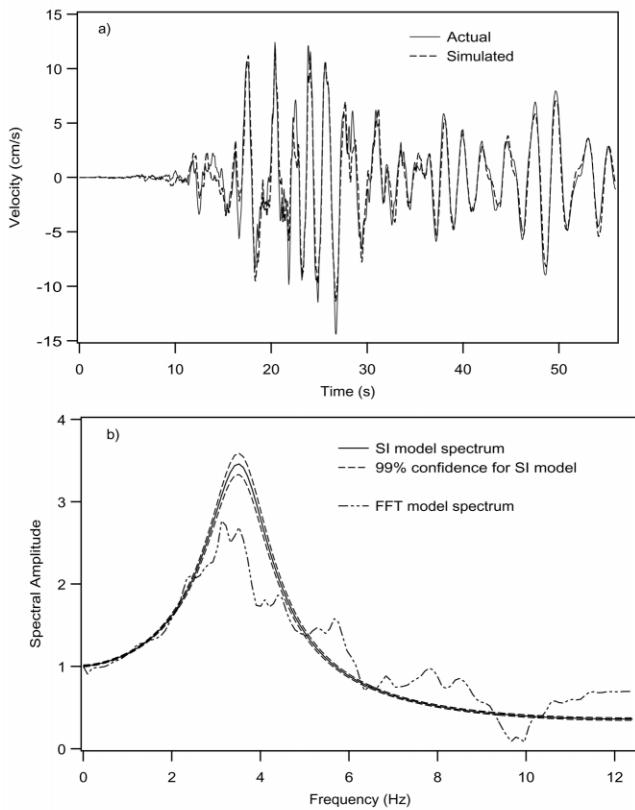


Fig. 6. (a) Time-invariant SI estimate of the 6 m to surface interval, Event 16. (b) Spectral realization of the SI model, with goodness-of-fit indicated by the 99% confidence interval. The FFT-based spectral estimate of the system behavior (spectral ratio) is shown for comparison.

(linear) model; the frequency response for this system is shown in Fig. 6b. The goodness-of-fit in the frequency domain is indicated by the 99% confidence interval given by the dashed lines, and the model is seen to have quite a small variance.

A useful method for analyzing changes in the system through time is to use a segmentation scheme that uses parallel recursive algorithms to find parametric changes within stated limits [34]. The soil parameters (damping ratio and shear stiffness) estimated for Event 16 indicate strain softening of the soil as compared to the baseline case. Fig. 7 presents the fundamental mode shear stiffness and damping estimates for the Event 16, 6 m-to-surface interval, and shows a change in the system that might be attributed to softening at about 22 s into the temblor, as per Zeghal et al. [17]. The change in system parameters correlates very well with the increase in pore pressure for this event, both indicating softening or non-linear behavior of the soils [47].

The question remains as to which model — time invariant (linear) or time-variant (non-linear) — better captures the essence of soil behavior. The linear model averages the system as compared to the segmented model, however both techniques result in consistent estimates. The recursive

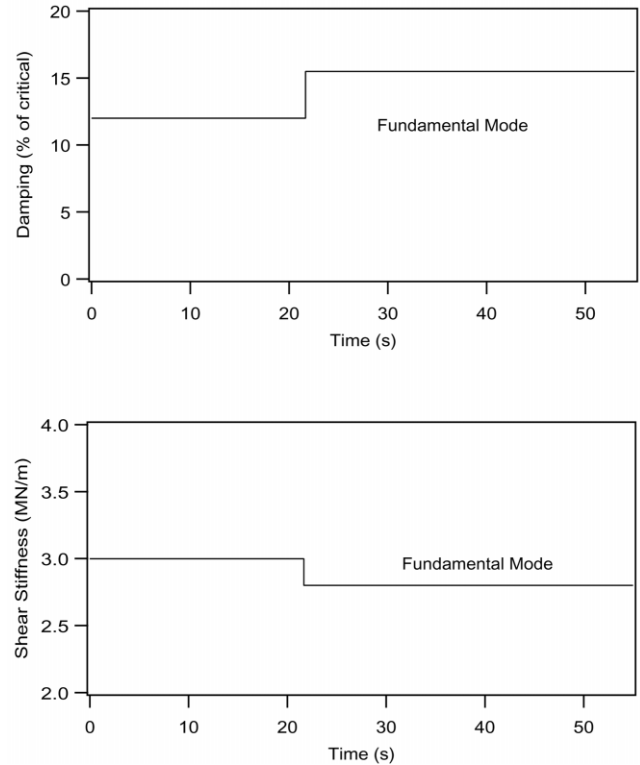


Fig. 7. Damping ratio and shear stiffness estimates for the 11–6 m interval, Event 16. Note change that can be attributed to softening at about 22 s into the temblor.

model may identify subtle changes in the soil system; however, the adequacy of the constant-parameter linear model to estimate the soil behavior indicates that the subtle change has little to no effect on the overall system behavior.

### 5.3. Events 7 and 8

Event 8 ( $M_L = 6.2$ ) is considered an aftershock of Event 7 ( $M_L = 6.2$ ) [1], so comparison of the results from these two events should cancel out any effects associated with hypocentral location and possibly source parameters allowing the effects of the magnitude of ground motions to be central. Although both events had very similar magnitudes, peak input acceleration for Event 7 was much greater than for Event 8 (0.21 vs. 0.03 g) as was the Arias intensity (652 vs. 139 m/s).

As expected, the estimated fundamental mode stiffness is lower when estimated from the Event 7 model, and damping ratio is higher, compared to values estimated for Event 8. However, the models for the low-energy Event 8 were able to capture the behavior of the various intervals well enough to accurately estimate the surface motions of the stronger Event 7. Fig. 8a compares the actual Event 7 surface layer output to the output estimated from the appropriate Event 8 filter model. The input to the model was the N–S 6 m velocity time history. The statistical confidence of this

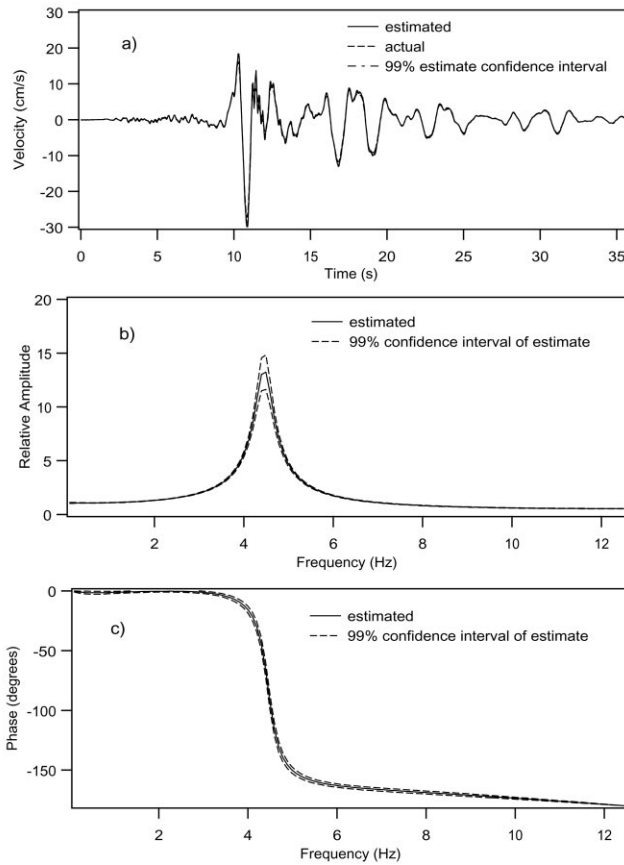


Fig. 8. Estimates of Event 7 behavior, DHB, 6 m to surface, made using Event 8 filter. (a) Actual, estimated, and estimated 99% confidence bounds for surface particle velocity. (b) Frequency domain visualization of soil interval filter and 99% confidence bounds for amplitude. (c) Frequency domain visualization of the soil interval filter and 99% confidence bounds for phase.

estimate is illustrated in the graphs shown in Fig. 8. This figure shows the 99% confidence interval in both the time (Fig. 8a) and frequency (Fig. 8b) domain. The results using the smaller-PGA filter give physically satisfying results. Our interpretation is that the change in soil behavior between Event 7 and 8 was small enough that the low-strain filter captured the essence of the soil layer (Event 7) behavior. The slight localized differences in soil properties between events is not significant enough to affect the overall system response.

5.4. Soil–structure interaction

Basic understanding of SSI predicts two effects of a structure sitting on a rigid foundation: (1) the shear stiffness of the soil/structure system would be higher than that of the structure on a non-rigid base; and (2) the damping ratio of the soil structure system would be larger than that of the structure on a rigid base [47]. These effects are in terms of the building rather than for the soil itself. Rollins and Seed [48] discuss the possible changes to soil response but come

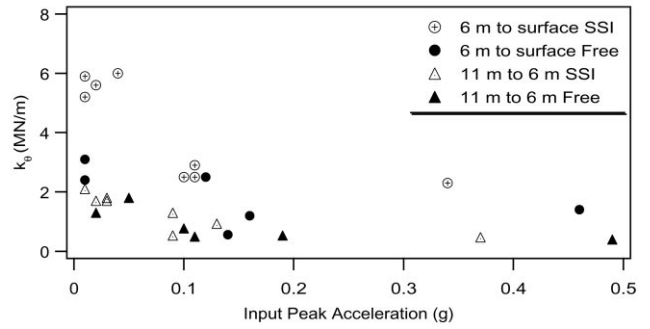


Fig. 9. Effect of soil–structure interaction (SSI) on interval fundamental mode shear stiffness as a function of peak input acceleration.

to no firm conclusions; neither did the extensive study on SSI for the Lotung site [11]. The unique data from Lotung allows comparison between the system parameters estimated at DHA and DHB by SI. The soil system parameters estimated for DHA (under the 1/4 scale containment structure) will likely be affected by the structure; therefore the estimated soil parameters should be considered to be “effective” soil system parameters including interactions of the structure.

Effective damping ratio and shear stiffness estimates for DHA are given in the subcolumn A in Table 2. The results are summarized graphically in Figs. 9 and 10 in comparison to the free field results (DHB), which are given in sub-column B in Table 2. Note that, the decrease in shear stiffness with increased PGA is much less pronounced for the results from DHA, the array under the model containment structure. For the 0–6 m interval, the shear stiffness shifts from 2.4 for Event 3 (PGA 0.01 g) to 0.6 MN/m for Event 7 (PGA 0.21 g). Note also that the stiffness values for the same events in the 0–6 m interval are lower under the structure compared to the free field values. This difference is hardly evident by the 6–11 m level; in fact, examination of the data for the 6–11, 11–17, 17–47 and 11–47 m intervals indicate that stiffness values are equivalent at DHA and DHB below 6 m (i.e. no SSI below 6 m depth). Other studies have predicted that the SSI would be evident to a depth of 17 m [11].

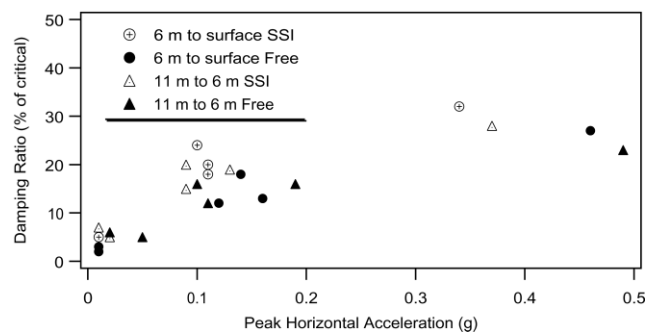


Fig. 10. Effect of soil–structure interaction (SSI) on interval effective viscous damping ratio as a function of peak input acceleration.

### 5.5. Meaning of the estimated damping ratio values

There is always a problem when discussing estimates of effective soil damping ratio since there is no hard and fast definition of the term, or theoretically proven absolute values against which to compare results. The ARMA parameters calculated in this study represent the weighting factors in the rational polynomial that can transfer input ground motions into output ground motions through convolution. The resultant weights are then mapped to an  $N$ -cascaded SDOF equation of motion; these lumped mass parameters can be represented in the frequency domain as poles and zeros, and in turn as stiffness and damping ratio.

Any linear (constant stiffness) model accounts for the actual non-linear stiffness behavior (resulting in load-displacement hysteresis loops) through the artifice of a complex damping term ( $i\eta$  or  $i\omega\eta$ ). The damping ratio used in either the linear wave propagation model or the lumped mass model do not represent actual, physical energy loss mechanisms, but are effective fitting parameters [49]. The results presented here, particularly those for the estimated viscous damping ratio, lead one to the conclusion that for the cases where the soil is behaving in an effectively linear fashion, the effect of effective damping is very small. Because damping exerts such a small effect on the system behavior, the model is very insensitive to a wide range of possible values as evidenced by the large range of damping values estimated from the inversions, most of which result in a very good forward simulation. This is not merely a function of using the lumped mass model, as the same conclusion is reached from a full time domain solution for the 1D wave equation [50], and from theory [51].

## 6. Conclusions

The results unambiguously indicate some changes in equivalent linear soil properties as a function of peak acceleration. Evidence of a decrease in soil interval fundamental mode shear stiffness and an accompanying general trend of increased effective viscous damping ratio with higher seismic accelerations are clear. The transition, while less pronounced with depth, consistently occurs above the peak acceleration of 0.07 g.

The changes in mechanical behavior, however, are not great enough to invalidate simulations made using linear models calibrated for mild shaking. Event 7 (0.21 g) was accurately modeled with a linear model derived from Event 8 (0.03 g), although time (acceleration history) dependent behavior is evident above 0.17 g. Event 16 (0.17 g) is modeled equally well with a linear (time-invariant) model as with a segmented time-variant model. Change in soil stiffness and damping as a function of peak acceleration is demonstrated at the site. It becomes obvious, however, that for the small degree of non-linearity exhibited at the Lotung site the linear models very effectively capture the essence of site response.

For the surface-6 m and 6–11 m intervals, the damping values are higher and the stiffness values lower for the large events as compared to the baseline case. This distinction is completely missing in the 17–47 m results, indicating that this interval does not show evidence of non-linear behavior during the studied suite of earthquakes. For the surface-6 m interval, the decrease in fundamental mode shear stiffness with increasing event energy is less pronounced under the 1/4 scale containment structure than in the free field. This soil-structure effect is increasingly diminished with depth and absent by the 17–47 m interval.

Comparison of the results of this study with previous work, considered with the inherent theoretical advantages of parametric modeling for transient and/or non-stationary time series such as earthquakes, suggest that SI is a powerful method for identifying shear stiffness and effective damping values for layers of earth materials when bore hole information is available.

## Acknowledgements

This paper was funded by NIST Contract no. 60NANB500074, with additional funding from NSF Young Investigator Award CMS94-57268 and from the NSF graduate fellowship program. We wish to thank the Electric Power Research Institute, in particular H.T. Tang, for making the data available through a Cooperative Research and Development Agreement with the National Institute of Standards and Technology. We also wish to thank Riley Chung and Ron Andrus, Structures Division, NIST, for providing technical support.

## References

- [1] Anderson DG. Geotechnical synthesis for the Lotung large-scale seismic experiment. Report TR-102362, Palo Alto: Electric Power Research Institute, 1993.
- [2] Anderson DG, Tang YK. Summary of soil characterization program for the Lotung large-scale seismic experiment. Proceedings: EPRI/NRC/TPC Workshop on Seismic Soil-Structure Interaction Analysis Techniques using Data from Lotung, Taiwan, Report NP-6154, 1989.
- [3] Glaser SD. Insight into liquefaction by system identification. *Géotechnique* 1997;00.
- [4] Glaser SD. Estimation of system damping at the Lotung site by application of system identification. GCR 96-700, Gaithersburg: NIST, 1996.
- [5] Glaser SD. System identification and its application to estimating soil properties. *Journal of Geotechnical Engineering* 1995;121(7):553–60.
- [6] Zeghal M, Elgamel A-W, Parra E. Identification and modeling of earthquake ground response — II. Site liquefaction. *Soil Dynamics and Earthquake Engineering* 1996;15:523–47.
- [7] Elgamel A-W, Zeghal M, Parra E, Gunturi R, Tang HT, Stepp JC. Identification and modeling of earthquake ground response — I. Site amplification. *Soil Dynamics and Earthquake Engineering* 1996;15:499–522.
- [8] Stewart JP, Fenves GL. System Identification for evaluating soil-structure interaction effects in buildings from strong motion

- recordings. *Earthquake Engineering and Structural Dynamics* 1998; 27:869–85.
- [9] Stewart JP, Fenves GL, Seed RB. Seismic soil–structure interaction in buildings. I: Analytical methods. *Journal of Geotechnology and Geoenvironmental Engineering* 1999;125:26–37.
- [10] Tang HT, Tang YK, Stepp JC, Wall IB, Lin E, Cheng SC, Lee SK, Hsiau HM. EPRI/TPC large-scale seismic experiment at Lotung, Taiwan. Proceedings: EPRI/ NRC/TPC Workshop on Seismic Soil–Structure Interaction Analysis Techniques using Data from Lotung, Taiwan, Report NP-6154, Palo Alto: EPRI, 1989.
- [11] Tang HT. Large-scale soil–structure interaction. Report NP-5513-SR. Palo Alto: Electric Power Research Institute, 1987.
- [12] Wen KL, Yeh YT. Seismic velocity structure beneath the SMART 1 array. *Bulletin of the Institute of Earth Science (Academia Sinica)* 1984;4.
- [13] Chang C-Y, Mok CM, Tang HT. Inference of dynamic shear modulus from Lotung downhole data. *Journal of Geotechnical Engineering* 1996;122(8):657–65.
- [14] Chang C-Y, Mok CM, Power MS. Analysis of ground response data at Lotung large-scale soil–structure interaction experiment site. Report NP-7306-M, Palo Alto: EPRI, 1991.
- [15] EPRI. Proceedings: EPRI/NRC/TPC Workshop on Seismic Soil–Structure Interaction Analysis Techniques using Data from Lotung, Taiwan, vol. 1 and 2, Report NP-6154., 1989.
- [16] Shen CK, Chan CK, Li XS, Yang HW, Ueng TS, Wu WT, Chen CH. Pore water pressure response measurements at Lotung site. Proceedings: EPRI/NRC/TPC Workshop on Seismic Soil–Structure Interaction Analysis Techniques using Data from Lotung, Taiwan, 2, EPRI Report NP-6154., 1987.
- [17] Zeghal M, Elgamal A-W, Tang HT, Stepp JC. Lotung downhole array: evaluation of soil non-linear properties. *Journal of Geotechnical Engineering* 1995;121(4):363–78.
- [18] Elgamal A-W, Zeghal M, Tang HT, Stepp JC. Evaluation of low-strain site characteristics using the Lotung seismic array. *Journal of Geotechnical Engineering* 1995;121(4):350–62.
- [19] Zeghal M, Elgamal A-W. Lotung site: downhole seismic data analysis. Report. Palo Alto: Electric Power Research Institute, 1993.
- [20] Seed HB, Idriss IM. Soil moduli and damping factors for dynamic response analyses. (EERC 70-10) Berkeley: University of California, 1970.
- [21] Elgamal A-W. Personal communication, 1998.
- [22] Chang C-Y, Mok CM, Power MS, Tang YK, Tang HT, Stepp JC. Development of shear modulus reduction curves based on Lotung down-hole ground motion data. Second International Conference on Recent Advances in Geotechnical Earthquake Engineering and Soil Dynamics, vol. 1, St. Louis, MO., 1991. p. 111–8.
- [23] Chang C-Y, Power MS, Tang YK, Mok CM. Evidence of non-linear soil response during a moderate earthquake. Proceedings of the 12th International Conference on Soil Mechanics and Foundation Engineering, vol. 3. Rotterdam: Balkema, 1989. p. 1927–30.
- [24] Chang C-Y, Mok CM, Power MS, Tang YK, Tang HT, Stepp JC. Equivalent linear versus non-linear ground response analyses at Lotung seismic experiment site. Proceedings of the 4th US National Conference on Earthquake Engineering, vol. 3 (EERI), 1990. p. 327–36.
- [25] Lee MKW, Finn WDL. Dynamic effective stress analysis of soil deposits with energy transmitting boundary including assessment of liquefaction: DESRA-2. Soil Mechanics Series no. 38, Vancouver, British Columbia, 1978.
- [26] Schnabel PB, Lysmer J, Seed HB. A computer program for earthquake response analysis of horizontally layered sites: SHAKE. Earthquake Engineering Research Center, Report 72-12. Berkeley, California, 1972.
- [27] Beck JL. Determining models of structures from earthquake records. Earthquake Engineering Research Laboratory, Report 78-01. Pasadena, California, 1978.
- [28] Ghanem RG, Gavin H, Shinozuka M. Experimental verification of a number of structural system identification algorithms. Technical Report NCEER-91-0024. Buffalo: National Center for Earthquake Engineering Research, 1991. p. 302.
- [29] Popescu TD, Demetriu S. Analysis and simulation of strong earthquake ground motions using ARMA models. *Automatica* 1990; 26(4):721–37.
- [30] Safak E. Analysis of recordings in structural engineering: adaptive filtering, prediction, and control. (Open-File Report 88-647). Menlo Park, CA: US Geological Survey, 1988.
- [31] Polhemus NW, Cakmak AS. Simulation of earthquake ground motions using autoregressive moving average (ARMA) models. *Earthquake Engineering and Structural Dynamics* 1981;9:343–54.
- [32] Hubral P, Treital S, Gutowski P. A sum autoregressive formula for the reflection response. *Geophysics* 1980;45(11):1697–705.
- [33] Kanasevich E. Time sequence analysis in geophysics. Edmonton, Alberta: University of Alberta Press, 1981.
- [34] Andersson P. Adaptive forgetting in recursive identification through multiple models. *International Journal of Control* 1985;42(11):1175–94.
- [35] Kalman R. A new approach to linear filtering and prediction problems. *Transactions of the ASME, Journal of Basic Engineering* 1960;3:35–45.
- [36] Pandit SM. Modal and spectrum analysis: data dependent systems in state space. New York: Wiley, 1991.
- [37] Kramer SL. Geotechnical earthquake engineering. Englewood Cliffs: Prentice-Hall, 1995.
- [38] Ljung LJ. System identification: theory for the user. Englewood Cliffs: Prentice-Hall, 1987.
- [39] Baise LG, Glaser SD. Consistency of ground motion estimates made using system identification. *Bulletin of the Seismological Society of America* 2000;90(4):993–1008.
- [40] Bohlin T. Model validation. In: Singh M, editor. Encyclopedia of systems and control. Oxford: Pergamon Press, 1987.
- [41] Pierce JR. An introduction to information theory. New York: Dover Press, 1980.
- [42] Shannon CE. Communication in the presence of noise. Proceedings of the Institute of Radio Engineers 1949;37:10–21.
- [43] Lin J-S. Extraction of dynamic soil properties using extended Kalman filter. *Journal of Geotechnical Engineering* 1994;120(12):2100–17.
- [44] Miller KS, Leskiw DM. An introduction to Kalman filtering with applications. Malabar, FL: Krieger, 1987.
- [45] Arias A. A measure of earthquake intensity. In: Hansen RJ, editor. Seismic design for nuclear power plants. Cambridge: MIT Press, 1970.
- [46] Dobry R, Oweis I, Ursua A. Simplified procedures for estimating fundamental period of a soil profile. *Bulletin of the Seismological Society of America* 1976;66(4):1293–321.
- [47] Tang YK, Tang HT. Lotung Large-Scale Seismic Test strong motion records, vol. 1-8. Report NP-7496, Palo Alto: Electric Power Research Institute, 1992.
- [48] Rollins KM, Seed HB. Influence of buildings on potential liquefaction damage. *Journal of the Geotechnical Engineering Division* 1990;116(2):165–85.
- [49] Lysmer J. Lectures on soil–structure interaction. Class handout, University of California, Berkeley, and personal communication, 1997.
- [50] Ching J-Y, Glaser SD. Time domain solution of 1D shear wave propagation in layered media and its application to predicting earthquake ground motions. *ASCE Journal of Geotechnical Engineering*, 2001 (provisionally accepted).
- [51] Gersch W. On the achievable accuracy of structural system parameter estimates. *Journal of Sound and Vibration* 1974;34(1):63–79.